JOURNAL OF CATALYSIS **163,** 245–254 (1996)
ARTICLE NO. 0325

Elemental Mapping of Heterogeneous Catalysts by Energy-Filtered Transmission Electron Microscopy

P. A. Crozier[1] and M. R. McCartney

Center for Solid State Science, Arizona State University, Tempe, Arizona 85287-1704

Received June 15, 1994; revised June 18, 1996; accepted June 19, 1996

A new technique for characterizing the distribution of elements on the nanometer scale over large areas is described for heterogeneous catalyst research. The method exploits recent developments in electron microscopy involving energy-filtered imaging and digital image recording. The new approach allows relatively large regions to be characterized in reasonable times. The technique is employed to study the elemental distribution in a NiCuCr catalyst.

© **1996 Academic Press, Inc.**

INTRODUCTION

Knowledge of catalyst composition and structure is critical to a fundamental understanding of the chemistry actually occurring during catalysis. From such information it is possible to determine which portions of the catalyst are active and how changes in catalyst synthesis and structure affect catalysis. Characterization is also vital to understanding the changes that occur in the structure and composition of a catalyst during use in the reactor (1).

In order to obtain a complete characterization of heterogeneous catalysts, it is important to have an accurate representation of their microstructure and nanochemistry. In many cases, there is a direct relationship between the microstructure of such systems and their catalytic properties (see Ref. (2) for numerous examples). Catalytic properties may depend on the presence and distribution of promoter elements and it is often essential for metal particles to be highly dispersed over the supporting substrate. Direct visualization of heterogeneous catalysts morphology on the nanometer scale can help in identifying critical factors in catalyst synthesis and design.

Heterogeneous catalyst performance degrades during use in the reactor and ultimately results in significant loss of activity. Many different mechanisms can be responsible for deactivation including particle sintering, coking, pore blocking, surface contaminant layers and promoter sintering (3). In many cases, understanding the detailed way in which deactivation occurs requires a microstructural representation of the system under study.

Modern transmission electron microscopy techniques provide powerful tools for direct visualization of the microstructure and chemistry of heterogeneous catalysts (4–6). High resolution electron microscopy (HREM) provides information on local crystallinity and can show up the overall morphology and surface structure that may be present in the supported metal catalyst systems (7). It is often the only technique capable of providing accurate information on stacking faults and other crystal defects that may play a critical role in defining catalysts properties (8). Annular dark-field imaging (ADF) with a scanning transmission electron microscope (STEM) has proven to be a powerful technique for showing the dispersion of small heavy-metal particles on light element oxide supporting materials (9). Energy dispersive X-ray spectroscopy (EDX) and electron energy-loss spectroscopy (EELS) allows one to determine the local elemental composition of regions. When combined with a modern STEM, these spectroscopies allow elemental information to be obtained from regions as small as 10 Å (10).

Characterizing the microstructural composition and elemental distributions of many modern industrial heterogeneous catalysts can be difficult because of the complex nature of their morphologies. There are often many different morphologies present within the catalyst and it is important to characterize relatively large areas and relatively large numbers of nanometer sized particles to obtain information that is statistically significant. Moreover, it is not uncommon for modern industrial catalyst to have six to ten elements in widely differing concentrations. In many cases, the catalyst may contain many elements of similar atomic number, making it difficult to distinguish different phases with conventional techniques.

The newly developed Zeiss 912 transmission electron microscope is fitted with an omega filter which allows electron images to be energy-filtered, i.e., electron energy-loss images can be formed on the microscope viewing screen. In electron energy-loss spectroscopy, electrons passing through the sample lose energy by exciting the atoms of the

[1] Correspondence and proofs to: P. A. Crozier, Center for Solid State Science, Arizona State University, Tempe, Arizona, 85287-1704; Tel: 602 965 2934; FAX: 602 965 9004.

0021-9517/96 $18.00
Copyright © 1996 by Academic Press, Inc.
All rights of reproduction in any form reserved.

catalyst (11). The spectrum of energy-losses contains ionization edges which result from inner-shell excitation and are characteristic of the elements of the catalyst. Energy-filtered imaging can be employed to carry out elemental mapping without the need for scanning techniques.

The Zeiss 912 machine has a nominal resolution of close to 3.8 Å and a Gatan slow-scan CCD camera is interfaced to the microscope for digitally recording two-dimensional electron images in a form that is well suited to processing and quantification (12, 13). Digital processing and analysis greatly facilitates elemental mapping with this technique and makes it feasible to perform quantification in reasonable time.

In this paper, the application of this new energy-filtering microscope to determining the elemental distributions in a NiCuCr catalyst is described. This system is typical of many complex industrial catalysts containing transition metal elements of similar atomic number and is an ideal test system for the present study. The metal can be present in both metallic and oxide states. Different methods for catalyst synthesis and exposure in a reactor may give rise to changes in the chemical composition of the catalyst that may not be apparent with conventional bright-field and dark-field imaging techniques. It is important to able to obtain elemental distributions over large areas in order to obtain statistically meaningful information. Moreover, such information should be available relatively quickly to make it feasible to compare the different microstructures from a series of catalysts exposed to different conditions.

After a brief discussion of sample preparation and the microscope column we demonstrate the technique by determining elemental maps for Ni, Cu, and Cr. Some of the limitations and precautions that must be exercised to obtain useful results are described. The technique shows great promise of enhancing our ability to determine more complete elemental distributions on the nanometer scale from complex industrial catalysts.

METHODS

Sample Preparation

NiCuCr catalyst are used in a number of different industrial processes and can be synthesized in many different ways. The purpose of the paper is not to describe the application or synthesis of the catalyst but rather to use this system to demonstrate the power of energy-filtered imaging to catalyst characterization. Extensive details of the synthesis and application of such catalyst can be found in the patent literature (14–16).

The particular system used here consisted of NiCuCr particles dispersed over gamma-alumina support. The support had a BET area of 200 m^2/g and a pore volume of 0.5 cc/g. The total metal loading was less than 50% with the Cu and Ni being present mostly in metallic form and the Cr being in the form of an oxide. The Cu/Ni and Cr/Ni atomic concentration ratios were approximately 15% and 3%, respectively.

The catalyst comes in the form of a pellet 1 mm in diameter. Thin samples were prepared for TEM by the technique of ultramicrotomy. In this technique, the pellet is vacuum impregnated with LR white resin and thin sections cut with a diamond knife to a nominal thickness of approximately 500 Å. Directly impregnating the pellet with resin should result in sections that preserve any morphological relationships that exists within the catalyst, provided that the sections are continuous (i.e., no material falls out during cutting). The sections are then coated with about 100 Å of carbon to prevent charging under the electron beam.

Figure 1 is a low magnification TEM image of the sample showing that the microtomy has resulted in good sections of large electron transparent regions. Each section is almost continuous, implying that the morphological relationships have been essentially preserved during the sample preparation. This image is typical of the microstructure found in this particular system and appears to be representative of the catalyst. Several distinct morphologies can be seen in this image. The large region in the center, marked A, consists of a large number of metal particles aggregated in close proximity to each other. The region marked B consists mostly of oxide support and EDX analysis shows that there is very little metal content within such regions. Region C corresponds to areas where many particles have been dispersed over the substrate. The image demonstrates that the dispersion of metal particles has not been uniform throughout the catalyst. It is also apparent from this image that there are thousands of metal particles within the field of view and that point by point elemental analysis using STEM techniques would be extremely tedious.

Energy-Filtered Imaging

A schematic diagram of the lower column of the ZEISS 912 energy-filtering microscope is presented in Fig. 2. The features of interest in this diagram are the magnetic omega filter spectrometer which is located after the first set of intermediate lenses.This spectrometer disperses the electrons into their different energy components and forms an energy-loss spectrum in the spectrometer exit plane. An energy-selecting slit is located in this plane to select the portion of the energy-loss spectrum that will be used to form the energy-filtered image on the microscope viewing screen or CCD detector. This slit is of variable width, allowing energy windows of different sizes to be selected. The CCD detector consists of 1024^2 pixels with each element being 24 μm in size. The detector has a linear dynamic range of just over 4000 and is adequate for quantitative measurement of energy-loss spectral intensities. The microscope can be operated in image mode, diffraction mode, or spectrum mode. When the microscope is run in spectrum mode, an

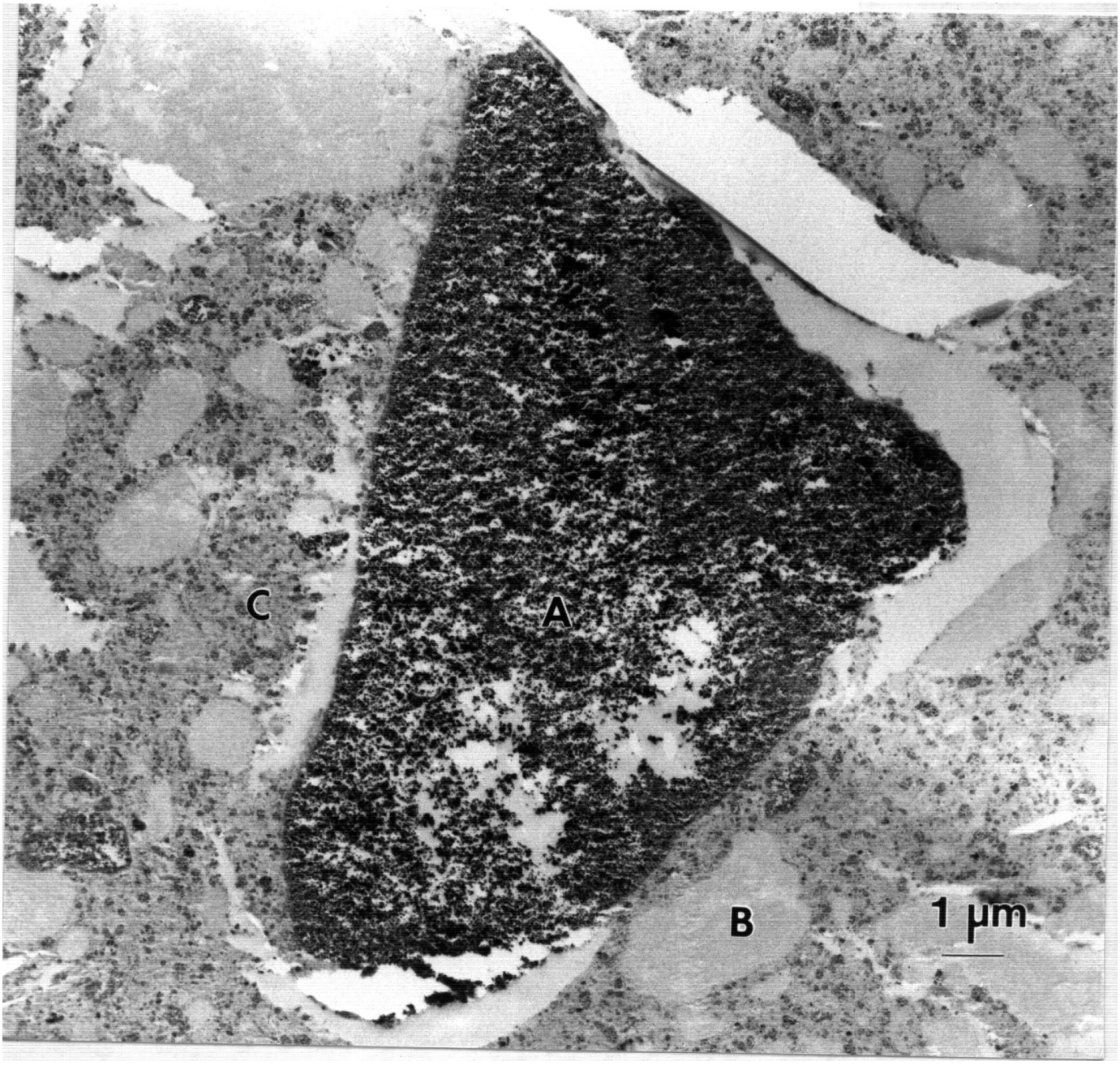

FIG. 1. Low magnification image of NiCuCr catalyst showing three different morphologies: Region A—high density metal particles, Region B—Al_2O_3 support with no metal particles, Region C—metal dispersed on Al_2O_3 support.

energy-loss spectrum can be acquired and processed using the CCD detection system.

The energy-loss spectrum consists of inner-shell ionization edges (which are characteristic of the elements present) superimposed on a non-characteristic background (see Fig. 3). Processing energy-loss spectra involves removing the background contribution and integrating the ionization edge intensity. For quantitative elemental mapping, it is necessary to acquire three energy-filtered images for processing. One image is recorded from the edge region and contains the ionization edges. The other two images are recorded from the pre-edge region and are used for the background extrapolation procedure. Background subtraction is usually achieved by fitting the form AE^{-r} to the region before the ionization edge and extrapolating this fitted background beyond the edge threshold as shown in Fig. 3. Details of this procedure are given elsewhere (17). Subtracting the background from the postedge image leaves an image which is proportional to the characteristic edge intensity.

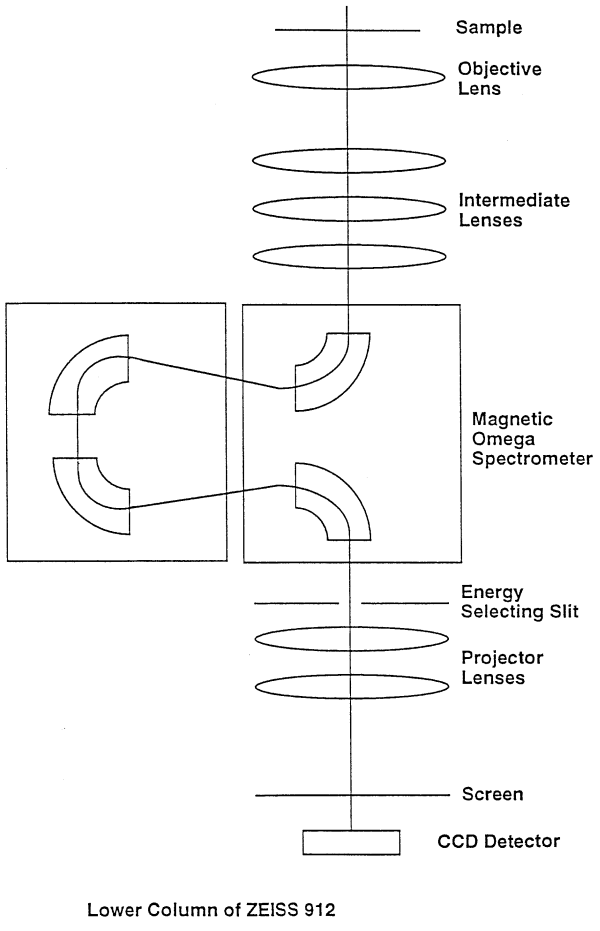

FIG. 2. Schematic diagram of lower column of Zeiss 912 showing omega filter, energy selecting slit, and CCD detector.

The image resulting from background subtraction is still not a true representation of the elemental distribution because contrast in TEM images arises from mass thickness and diffraction effects. The diffraction contrast is particularly important in heterogeneous catalyst systems which usually consist of many small crystals in differing orientations. In order to obtain a signal that is not strongly dependent on thickness or diffraction effects, it is necessary to normalize this characteristic signal map using a conventional TEM bright-field image recorded close to Gaussian focus. The bright-field image is acquired under identical conditions with the energy window set equal to the value used for the energy filtering (18). This normalization process effectively removes most of the diffraction and mass thickness contrast and leaves an image which is a true representation of the elemental distribution within the region of interest. It is possible to convert this intensity distribution into the number of atoms per unit area by employing either theoretical ionization cross sections or through use of empirical *k*-factors (18–20) from standards. In this case, theoretical ionization cross sections are employed to determine absolute elemental concentrations.

Practical Details

The active area of the CCD array is only 2.5 cm^2 in size. In order to sample a reasonably large area of the specimen it is necessary to operate the microscope in a relatively low range of magnification. In this instance, the microscope magnification was set to 5000X giving a sampled region 2.5 μm across. One million pixels of information are sampled from this area with a pixel size of approximately 25 Å. This operating condition is a reasonable compromise between large area sampling and moderate spatial resolution. In the images presented here, the resolution is limited to approximately 50 Å.

Some consideration should be given to the width, Δ, of the energy-selecting slit. It is desirable to choose a slit width which is large enough to give reasonable counting statistics and average out some of the chemical oscillations that appear close to the ionization edge threshold (the so-called near-edge structure). However, for edges that are close together, it is also important to chose a small enough value of Δ to avoid significant edge overlap or significant background extrapolation errors are likely to be introduced. For the experiments described here, a value of $\Delta = 25$ eV is a reasonable compromise between these two competing factors. Further details on acquisition conditions are given in (17).

It takes approximately 0.1 s to acquire the bright-field image and between 1–10 s to acquire each energy-filtered image for the different ionization edges. An acquisition time of 10 s yielded adequate statistical precision for all edges out to 1000 eV energy loss (giving elemental information on Ni, Cu, and Cr).

During the course of image acquisition, some sample drift can occur due to local heating of the embedding resin. The drift that occurred between images was removed using cross-correlation techniques to align all the images to the

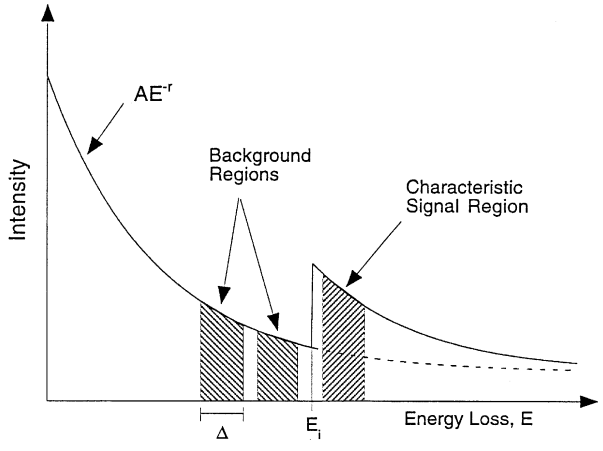

FIG. 3. Schematic diagram of energy-loss spectrum showing characteristic signal and three regions of spectrum employed to generate elemental maps. The ionization edge energy is E_i and each region of the spectrum is of width Δ.

bright-field image. The analysis procedures used to determine elemental concentrations by energy-loss spectroscopy are only valid in regions of the sample thin enough to ensure that plural inelastic scattering is not significant (21, 22). The contribution to a spectrum from plural scattering depends on the sample thickness t and the inelastic mean free path λ. It is conventional to employ a quantity known as the scattering parameter t/λ (defined as the thickness expressed in terms of the mean free path) to determine the contribution of plural scattering to an energy-loss spectrum. The contribution from plural scattering is small for t/λ values of less than 0.5, although elemental information can be extracted from regions with t/λ values of close to 1.

Values of t/λ for every pixel in the map can be obtained by acquiring and processing a pair of bright-field images. Details of this procedure are given elsewhere (17). The analysis shows that t/λ is less than unity over most of the regions of interest and demonstrates that microtomy is an excellent technique for preparing large uniform thin areas of NiCuCr catalyst suitable for elemental mapping by energy-loss spectroscopy.

RESULTS

Figure 4 is part of a typical energy-loss spectrum showing the Ni L_{23} edge at 855 eV from a region of type A morphology (a high density of particles). Ni is present in high concentration in this catalyst and consequently the signal-to-background ratio for the Ni edge is very good. The images shown in Fig. 5 show the Ni elemental map, from the type A morphology region, together with a series of three component images used to generate the Ni map. Figure 5a is the bright-field image obtained using a slit width of 25 eV which allows electrons which have lost energy in the range 0–25 eV to reach the image plane. The high contrast in the bright-field image is the result of variations in thickness and strong diffraction effects, with the most strongly diffracting crystals appearing dark. This bright-field image is used in the normalization procedure to compensate for the effects of mass thickness and diffraction. Figure 5b and c are energy-filtered images recorded using different parts of the energy-loss spectrum shown in Fig. 4. Figure 5b is taken just before the Ni L_{23} edge with the energy range 820–845 eV and Fig. 5c is taken just after the L_{23} edge with the energy range 855–880 eV.

It is helpful to discuss the interpretation of the energy filtered image present in Fig. 5. All energy-filtered (or inelastic) images are dark-field images in which the sample shows as light or gray contrast and the vacuum shows as black. Comparison of the images of Fig. 5 shows that the most significant difference is that the bright-field (or elastic) image of Fig. 5a shows contrast reversal with respect to 5b and 5c. The other major difference is that the energy-filtered images have much lower intensity than the bright-field image. This is because the probability for inelastic scattering into the energy window used to form the image is very small.

Inspection of Figs. 5b and 5c shows that, although both are dark-field images, the nature of the contrast is quite different. The background image (Fig. 5b) is of lower intensity because the region before the Ni L_{23} edge is about a factor of 2–3 weaker than the edge region (see Fig. 4). The contrast in this image is produced mostly by variation in the total scattering power of the sample (which depends on sample thickness and the average atomic number). Figure 5c is formed using the Ni L_{23} ionization edge and the intensity of those regions of the image rich in Ni appear brighter compared to Fig. 5b.

Although Fig. 5c shows enhanced sensitivity to Ni it is not strictly an elemental map. To obtain an elemental map the image must be corrected for the background contribution and normalized to the bright-field image as discussed in the previous section. The resulting Ni distribution is shown in Fig. 5d. The elemental map is essentially a dark-field image in which Ni rich regions show up with bright contrast and everything else is dark. Although Fig. 5d is rather noisy the distribution of intensity is directly proportional to the number of Ni atoms per unit area. The spatial resolution is about 5 nm in this case.

Figure 6 is a series of images used to identify the location of the Cr. In this case, the Cr L_{23} edge at 575 eV is used to perform the elemental mapping. Energy filtered images are acquired with the Cr L-edge at 575 eV and for background subtraction at 545 eV (see Figs. 6b and c).

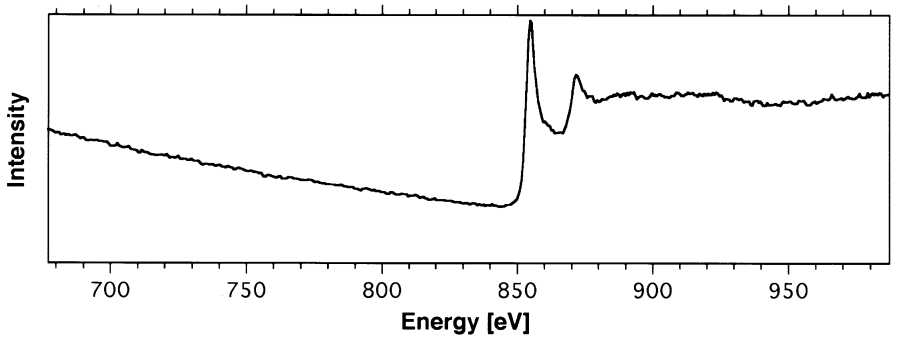

FIG. 4. A typical energy-loss spectrum from a region of catalyst of type A morphology.

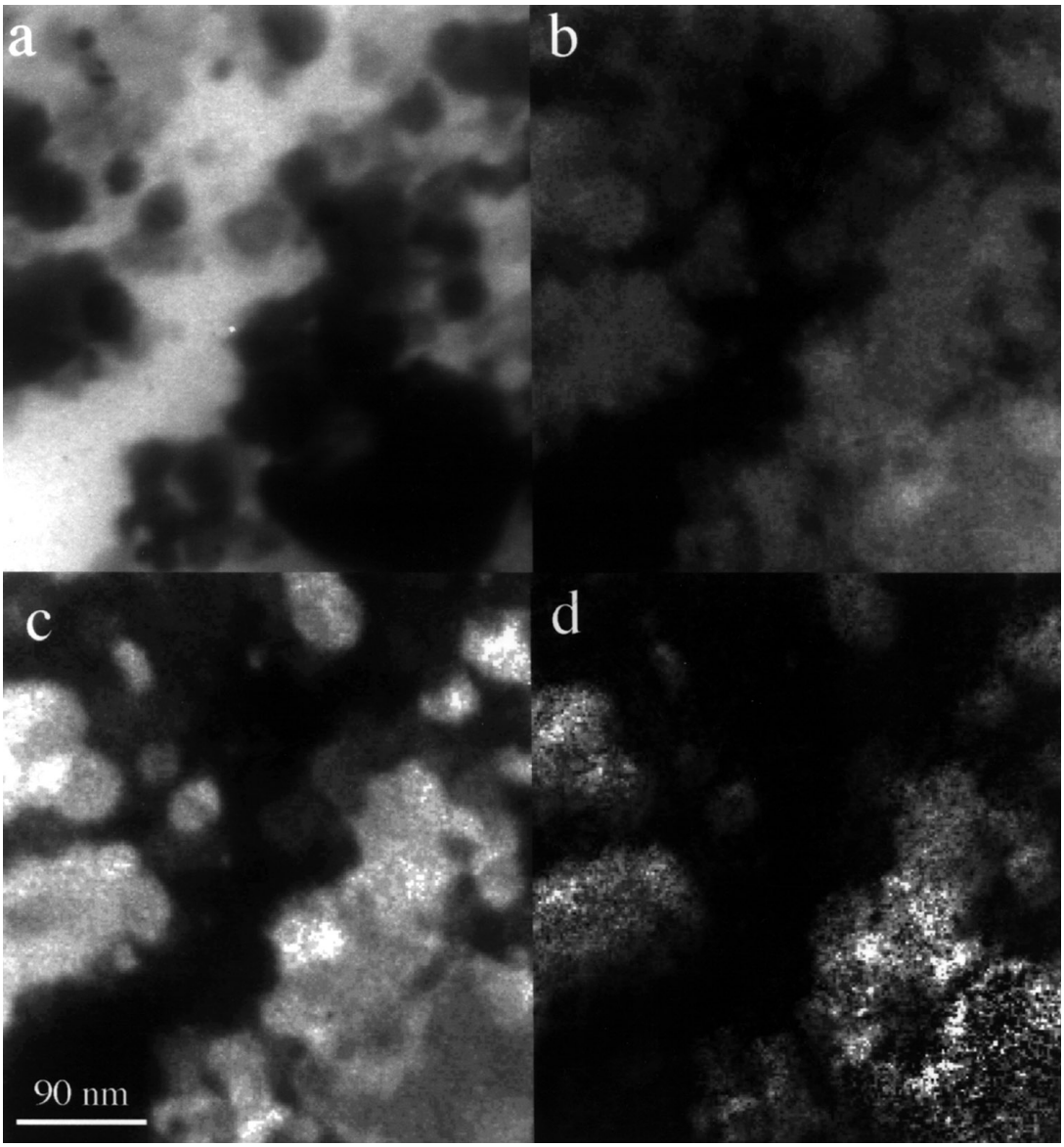

FIG. 5. Series of component images and resultant Ni distribution determined by image analysis and reduction: (a) bright field image recorded with $\Delta = 25$ eV; (b) one of the two background images recorded at 820 eV loss used in determination of the background; (c) image recorded at 855 eV loss which contains Ni sensitive signal, (d) Ni distribution obtained for this system.

Inspection of Figs. 6b and 6c reveals that in this case the differences between the post- and pre-edge images is less marked compared to the case for Ni because Cr is a minor component of the catalyst. The images are less noisy than the Ni energy-filtered images because the intensity of the energy-loss spectrum is stronger at the Cr L-edge compared to the Ni L-edge. However, careful comparison of 6b and 6c reveals that a number of small particles are bright in 6b suggesting that these particles are rich in Cr. The image obtained by subtracting 6b from 6c and normalizing to the bright-field image is shown in Fig. 6d and shows the distribution of Cr-rich particles. Comparing Figs. 6d and 6c and 5d indicates that the Cr is in the form of particles 100–200 Å in size decorating the surface of the Ni particles. Earlier unpublished work showed that the Cr particles are oxidized although the oxidation state was not determined.

The elemental maps shown in Figs. 5 and 6 are quantitative representations of the Cr and Ni distributions with a spatial resolution of about 5 nm over a sampled area of about 400×400 nm. One advantage of energy-filtered imaging is that much larger areas of the specimen can be mapped in acceptable times with no loss in spatial resolution. Figure 7 shows the bright-field image and elemental maps obtained using the full area of the CCD detector. In this case, each image consists of 1024^2 pixels, permitting a much larger area of the catalyst to be sampled. The bright-field image illustrates the large number of particles present in this part of the catalyst. Figure 7b is a composite color

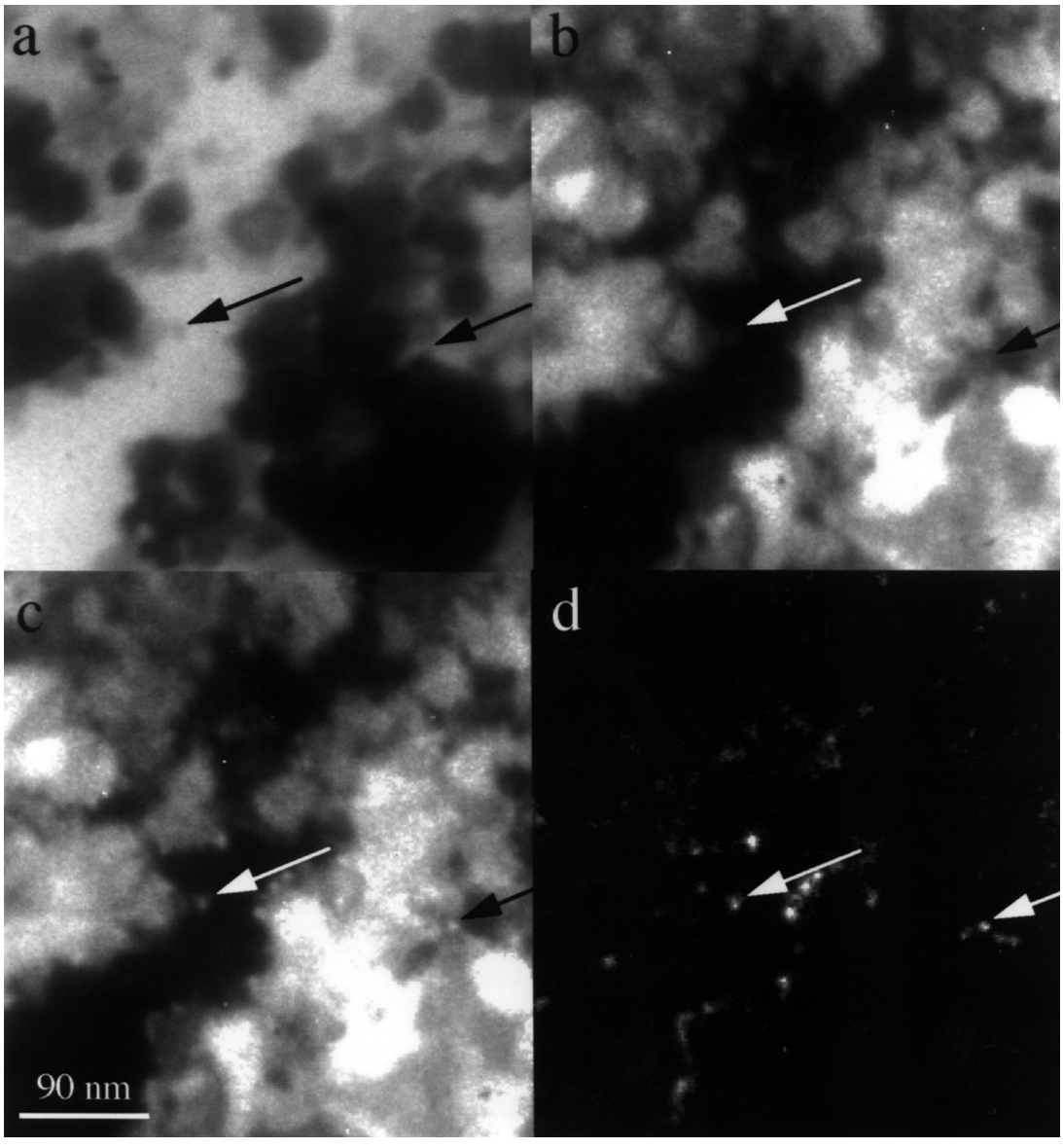

FIG. 6. Series of component images and resultant Cr distribution determined by image analysis and reduction: (a) bright field image recorded with $\Delta = 25$ eV; (b) a pre-edge images recorded at 545 eV loss used in determination of the background; (c) image recorded at 575 eV which contains the Cr L-edge; (d) Cr distribution obtained for this system.

elemental map obtained by overlaying the individual Cr, Ni, and Cu maps. The color representation allows spatial relationships between the three elements to be more easily seen. Figure 7b shows that the Ni and Cr elemental distributions are similar to those noted previously for Figs. 5 and 6. From inspection of Fig. 7b, it is clear that there are a few local areas, where the Cu signal is high, suggesting that Cu-rich phases have formed. However, in most of the image, the Cu signal is weak but not zero and strongly correlates with the Ni map. Questions of interest concern the relative amounts of Cu associated with the Cu-rich precipitates versus the amount associated with Ni.

To answer these questions it is necessary to determine the approximate accuracy of the quantification procedures. Although the maps provide information on the local variation of elements, it is also possible to integrate the total intensity in both the Ni and Cu maps to determine the average Cu/Ni concentration ratio for the total area of the image. We do not expect significant segregation of the elements into different regions of the pellet in the unused catalyst. We also believe that the regions selected for this analysis are fairly typical of the catalyst pellet. It then follows that if a sufficiently large area is analyzed, the average Cu/Ni concentration ratio should equal the bulk value. Integrating the intensity in the Cu and Cr maps gives a Cu/Ni ratio of 0.18 which is close to the bulk value of 0.15. This result indicates that the quantification procedures are reliable and should be accurate to within 20%.

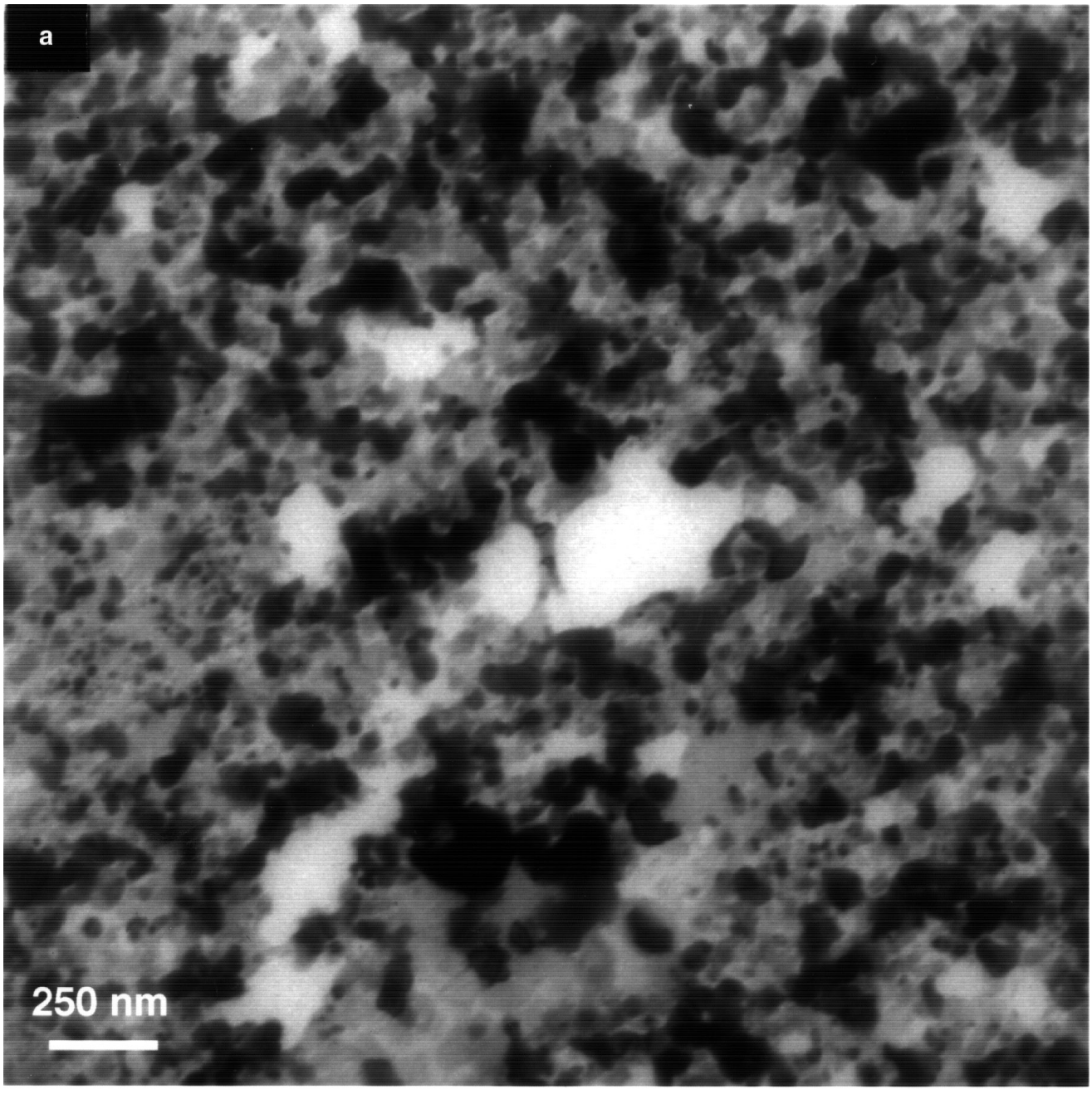

FIG. 7. (a) Large area bright-field image; (b) composite color elemental map showing the distribution of Ni (blue), Cu (green), and Cr (red).

Quantitative high spatial resolution analysis can be carried out simply by summing the intensity of pixels in each map over the appropriate area, i.e. the particle of interest. Details of this procedure are given in Ref. (17). Analysis of the individual Cu-rich particles shows that Cu/Ni ratio is close to unity in some of the particles. Away from the Cu-rich particles, the Cu/Ni ratio was consistently found to be 0.16–0.17, which compares to the average experimental value 0.18 value quoted above for the entire image. Our analysis suggests that about 90% of the Cu is contained in the regions of the catalyst with low Cu/Ni concentration. Approximately 10% of the Cu is located in the precipitates with equal amounts of Cu and Ni catalyst.

The average Cr/Ni ratio determined from the elemental maps by summing over the entire image, as described above, was 0.008 which is a factor of 4 lower than the bulk value of 0.03. Several factors account for the measured discrepancy between the two values. First, most of the Cr particles are observed dispersed over the surface of the Ni particles and most of the Ni particles are larger than 500 Å (which is the

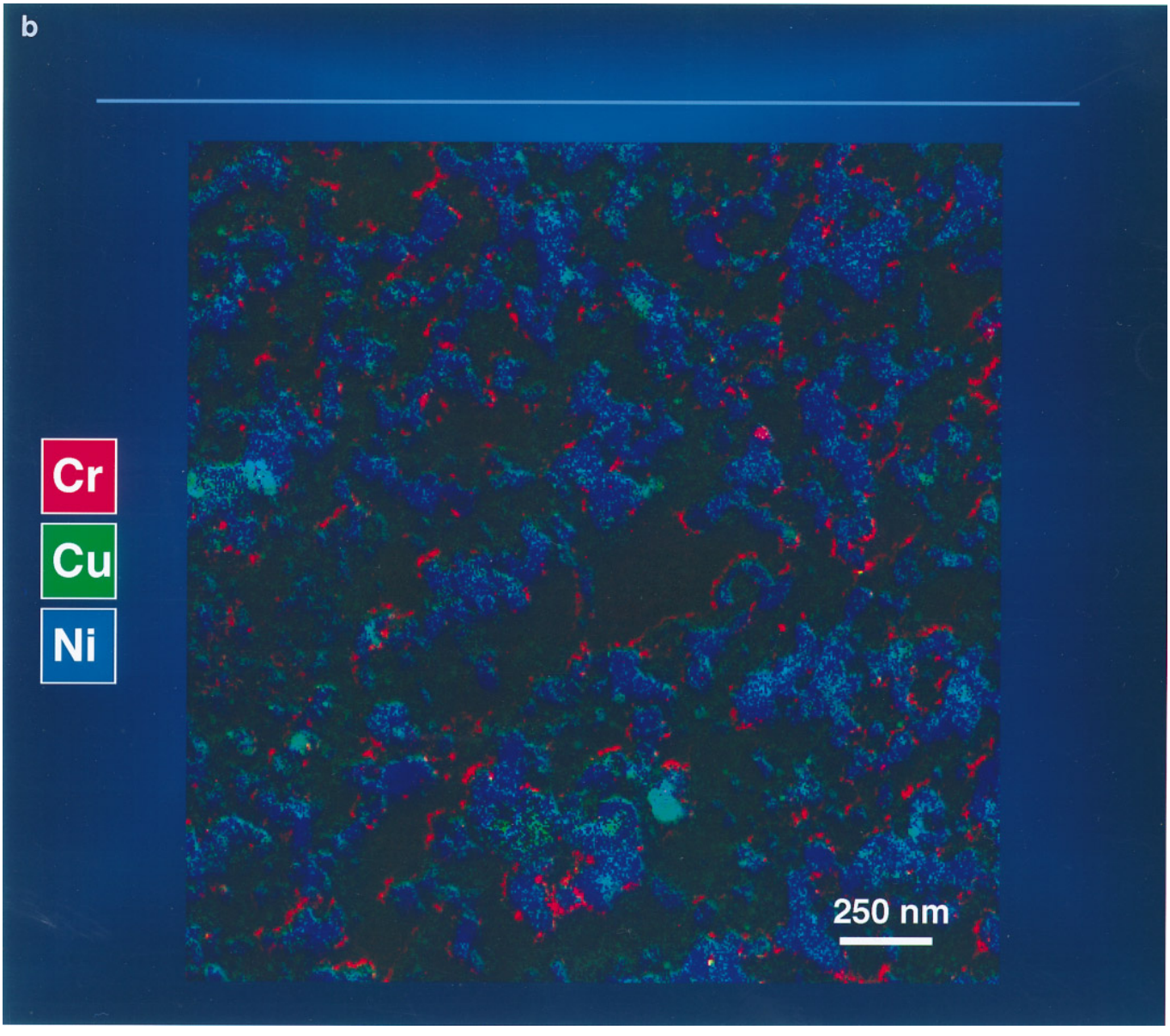

FIG. 7—Continued

nominal sample thickness). Under such conditions, the upper and lower sections of each Ni particle may be removed during sample preparation, leaving only the middle section in the TEM sample. This will reduce the surface layer contribution and thus lower the number of Cr particles that can be detected. By considering the geometry of sample preparation, it can be shown that the Cr/Ni will be reduced by approximately 60% relative to the bulk analysis values.

Second, the simple subtraction procedure used to remove the Cr background will always overestimate the background and thus reduce the magnitude of the Cr signal. This method of processing the Cr data will always result in the Cr signal being underestimated. The magnitude of this error will increase with decreasing Cr signal-to-background ratio and suppress the signal in the middle of thicker Ni particles, essentially producing profile maps of Cr. One final reason for the discrepancy could be that the Cr may not all be in the form of small precipitates. Some of the Cr may be in the form of surface layers. It is very likely that Cr present in this form may be below the detection limit of this mapping technique.

COMPARISON OF EFEM WITH CONVENTIONAL STEM EDX MAPPING

Elemental mapping with a dedicated STEM can also be employed to determine the complete distribution of elements with nanometer resolution in the catalyst. In

this technique, a small, high brightness electron probe produced by a field emission gun (FEG) electron source is scanned over the area to be mapped (23, 24). The intensity of elemental peaks in the EDX or EELS spectrum for each point in the sample is measured in order to build up the elemental image.

EDX is a very robust and versatile elemental analysis technique that can be used on thicker samples. The energy-filtering technique requires the use of very thin samples in order to avoid plural scattering. EDX spectra are usually easier to quantify and, in general, the technique is more sensitive in many materials applications.

However, one problem with STEM mapping by EDX is that the technique tends to be a rather slow process. Even though the FEG is a high brightness electron source, the total current available from such a source is low (on the order of 10 nanoamps). Consequently, high spatial resolution EDX mapping is usually performed over a relatively small area and it is often unclear if the map is truly representative of the entire catalyst. Typically, a 128^2 pixel map can take 30–60 min and significant specimen drift can occur within this time.

The Zeiss EFEM has a LaB_6 electron source which yields total electron beam currents a factor of 100 higher than those available using field emission sources. The much higher beam current available on this machine makes it well suited for performing large area mapping in reasonable time thus providing elemental distributions over statistically more meaningful areas. For the one million pixel elemental maps shown in Fig. 7, the total time needed to acquire the images for each map was 30 s. The ability to survey large areas at moderate resolutions (2–10 nm) in a reasonable time is the main advantage that EFEM offers over conventional EDX STEM analysis. This advantage can be significant when studying the elemental distributions in complex catalytic systems.

CONCLUSION

A new approach for generating elemental maps with nanometer spatial resolution has been demonstrated for heterogeneous catalysts characterization. This approach combines conventional TEM with energy-filtered imaging and digital image recording. The use of an LaB_6 electron source allows a factor of 100 increase in the number of sampling points in each map compared to STEM techniques with comparable spatial resolution. This allows substantially larger and more representative areas of the catalyst to be studied with nanometer spatial resolution in reasonable times. Many elements can be mapped out in sequence in order to build up a multielement representation in heterogeneous catalysts with complex morphologies.

Quantitative elemental concentration ratios determined from an unused NiCuCr catalyst indicate that the technique has an accuracy of better than 20%. For this particular system, Cu always correlates with Ni, although two different phases appear to be present. About 90% of the Cu was found in regions with a measured Cu/Ni concentration ratio of about 0.16. About 10% of the Cu was found in regions with a measured Cr/Ni concentration ratio close to unity. The Cr was found to exist in the form of small oxide particles 100–200 Å in size decorating the surface of the Ni particles. These results demonstrate the power of energy-filtered imaging for heterogeneous catalyst characterization.

ACKNOWLEDGMENTS

The authors thank Dr. Eugene Nebesh of Engelhard Corporation for valuable discussions. This work was supported by Arizona State University HREM Industrial Associates Program and made use of the Center for HREM supported by NSF Grant DMR-91-15680.

REFERENCES

1. Thomas, J. M., and Thomas, W. J., "Introduction to the Principles of Heterogeneous Catalysis," Academic Press, New York, 1967.
2. Treacy, M. M. J., Thomas, J. M., and White, J. M. (Eds.), "Microstructure and Properties of Catalysts," Vol. 111, Mater. Res. Soc., New York, 1988.
3. Baker, R. T. K., and Chludzinski, J. J., *J. Catal.* **64**, 464 (1980).
4. Baker, R. T. K., *Catal. Rev. Sci. Eng.* **19**, 161 (1979).
5. Mustard, D. G., and Bartholomew, C. H., *J. Catal.* **67**, 186 (1981).
6. Harris, P. J. F., Boyes, E. D., and Cairns, J. A., *J. Catal.* **82**, 127 (1983).
7. Datye, A. K., and Smith, D. J., *Catal. Rev.-Sci. Eng.* **34** (1&2), 129 (1992).
8. Lobo, R. F., Pan, M., Chan, I., Li, H-X., Medrud, R. C., Zones, S. I., Crozier, P. A., and Davis, M. E., *Science* **262**, 1543 (1993).
9. Treacy, M. M. J., and Rice, S. B., *J. Microsc.* **156**, 211 (1989).
10. Lyman, C. E., *Mater. Res. Soc. Symp. Proc.* **62**, 403 (1986).
11. Mayer, J., *in* "Proc. Electron Microscopy Society of America," p. 1198, San Francisco Press, San Francisco, 1992.
12. de Ruijter, W. J., and Weiss, J. K., *Rev. Sci. Instr.* **63**(10), 4314 (1992).
13. Pan, M., and Crozier, P. A., *Ultramicroscopy* **48**, 332 (1994).
14. Moss, P. H., and Godfrey, N. B., U.S. Patent No. 3,151,115 (1964), "Method for the Simultaneous Production of Acyclic and Polycyclic Amines."
15. Larkin, J. M., and Renken, T. L., U.S. Patent No. 4,766,245 (1988), "Process for the Preparation of Polyoxyalkylene Polyamines."
16. Zimmerman, R. L., and Larkin, J. M., U.S. Patent No. 5,003,107 (1991), "Catalytic Method for the Reductive Amination of Poly(oxytetramethyle) Glycols."
17. Crozier, P. A., *Ultramicroscopy* **58**, 157 (1995).
18. Egerton, R. F., *Ultramicroscopy* **3**, 242 (1978).
19. Egerton, R. F., *Ultramicroscopy* **4**, 169 (1979).
20. Egerton, R. F., "Electron Energy-Loss Spectroscopy in the Electron Microscope," Plenum, New York, 1986.
21. Crozier, P. A., *Philos. Mag. B* **61**(3), 311 (1990).
22. Egerton, R. F., *Ultramicroscopy* **6**, 297 (1981).
23. Leapman, R. D., and Fiori, C. E., "Analytical Electron Microscopy—1987" (D. C. Joy, Ed.), p. 184. San Francisco Press, San Francisco, 1988.
24. Statham, P. J., and Jones, M., *Scanning* **3**, 168 (1980).